Structural Basis for Inhibition of Mammalian Adenylyl Cyclase by Calcium[†]

Tung-Chung Mou,[‡] Nanako Masada,[§] Dermot M. F. Cooper,[§] and Stephen R. Sprang*[,‡]

Center for Biomolecular Structure and Dynamics and Division of Biological Sciences, The University of Montana, Missoula, Montana 59812, and Department of Pharmacology, University of Cambridge, Cambridge CB2 1PD, United Kingdom

Received November 17, 2008; Revised Manuscript Received February 24, 2009

ABSTRACT: Type V and VI mammalian adenylyl cyclases (AC5, AC6) are inhibited by Ca^{2+} at both sub- and supramicromolar concentration. This inhibition may provide feedback in situations where cAMP promotes opening of Ca^{2+} channels, allowing fine control of cardiac contraction and rhythmicity in cardiac tissue where AC5 and AC6 predominate. Ca^{2+} inhibits the soluble AC core composed of the C1 domain of AC5 (VC1) and the C2 domain of AC2 (IIC2). As observed for holo-AC5, inhibition is biphasic, showing "high-affinity" ($K_i = \sim 0.4\ \mu M$) and "low-affinity" ($K_i = \sim 100\ \mu M$) modes of inhibition. At micromolar concentration, Ca^{2+} inhibition is nonexclusive with respect to pyrophosphate (PP_i), a noncompetitive inhibitor with respect to ATP, but at $>100\ \mu M$ Ca^{2+}, inhibition appears to be exclusive with respect to PP_i. The 3.0 Å resolution structure of Gαs·GTPγS/forskolin-activated VC1:IIC2 crystals soaked in the presence of ATPαS and 8 μM free Ca^{2+} contains a single, loosely coordinated metal ion. ATP soaked into VC1:IIC2 crystals in the presence of 1.5 mM Ca^{2+} is not cyclized, and two calcium ions are observed in the 2.9 Å resolution structure of the complex. In both of the latter complexes VC1:IIC2 adopts the "open", catalytically inactive conformation characteristic of the apoenzyme, in contrast to the "closed", active conformation seen in the presence of ATP analogues and Mg^{2+} or Mn^{2+}. Structures of the pyrophosphate (PP_i) complex with 10 mM Mg^{2+} (2.8 Å) or 2 mM Ca^{2+} (2.7 Å) also adopt the open conformation, indicating that the closed to open transition occurs after cAMP release. In the latter complexes, Ca^{2+} and Mg^{2+} bind only to the high-affinity "B" metal site associated with substrate/product stabilization. Ca^{2+} thus stabilizes the inactive conformation in both ATP- and PP_i-bound states.

The nine membrane-bound mammalian adenylyl cyclase (AC)[1] isoforms and a soluble AC (sAC) catalyze the conversion of ATP to the intracellular second-messenger cAMP and pyrophosphate (PP_i) (*1, 2*). Biochemical and crystallographic studies show that this enzymatic process requires Mg^{2+} or Mn^{2+} as cofactors (*3*−*5*). Membrane-bound ACs are activated by the stimulatory G-protein α subunit (Gαs) and other regulatory molecules (*1, 6, 7*). The catalytic activity of several ACs is profoundly influenced by submicromolar Ca^{2+} (*8, 9*). At resting physiological concentration of ∼100 nM (*10*), calcium ions stimulate type I and type VIII isoforms of AC but inhibit types V and VI. These isoforms, which are differentially expressed in tissues, integrate the effects of calcium- and cAMP-mediated signaling to control diverse cellular functions (*11*−*13*). Calmodulin mediates the calcium stimulation of both type I and type VIII AC and could contribute to mechanisms of learning and memory (*14*−*17*). Type III AC is regulated by calmodulin and CAM kinase II (*18, 19*), and type IX is subject to calcium inhibition through the action of calcineurin (*20*). The two calcium-inhibited ACs (types V and VI) are highly expressed in cardiovascular tissue and have been proposed to be key negative feedback regulators of cardiac rhythmicity (*21*−*23*). At high (>10 μM) concentration Ca^{2+}inhibits all mammalian AC isoforms (*9, 11, 24, 25*).

The catalytic site of AC, as for all class III cyclases, resides at the interface of two homologous cyclase homology domains (CHD) (*26*). The model for the prototypical AC catalytic core is derived from crystal structures of the complex formed by the C1 CHD domain from AC5 and the C2 CHD domain from AC2 (VC1:IIC2) bound to two activators, forskolin (FSK) and GTPγS-activated Gαs (*27*). Structural studies of activated VC1:IIC2 complexes bound to substrate analogues show that the active site of AC contains two Mg^{2+} (or Mn^{2+}) sites, designated "A" and "B", that must be occupied for catalytic activity (*5*). Upon binding to potent substrate analogues, AC undergoes a transition from an "open" to a "closed" conformation by moving several structural elements in both CHDs toward the catalytic site. In the catalytically active conformation, both divalent metal ions coordinate with the substrate and with two conserved aspartic acid residues, Asp-396 and Asp-440 (residue numbers refer to AC5) in the C1 domain. The metal ion in site

[†] This work was supported by NIH Grant R01-DK46371 (S.R.S.) and Wellcome Trust Grant RG31760 (D.M.F.C.). D.M.F.C. is a Royal Society Wolfson Research Fellow.

* To whom correspondence should be addressed. Phone: (406) 243-6028. Fax: (406) 243-4227. E-mail: Stephen.sprang@umontana.edu.

[‡] The University of Montana.

[§] University of Cambridge.

[1] Abbreviations: AC, adenylyl cyclase; mAC, mammalian membrane-bound adenylyl cyclase; VC1 and IIC2, the N- and C-terminal catalytic domains from canine AC5 and rat type II AC, respectively, expressed as soluble proteins; Gαs, stimulatory G-protein for AC; FSK, forskolin; MP-FSK, 7-acetyl-7-[*O*-(*N*-methylpiperazino)-γ-butyryl]forskolin; sAC, soluble, bicarbonate-activated adenylyl cyclase; EC_{50}, molar concentration of Ca^{2+}, which produces 50% of the maximum AC activity; [Ca^{2+}], calcium concentration; ATPαS, adenosine 5′-[α(R_p)-thio]triphosphate; Ap(CH)pp, α,β-methyleneadenosine 5′-triphosphate; GTPγS, guanosine 5′-[γ-thio]triphosphate; PP_i, pyrophosphate; 2′-d-3′-AMP, 2′-deoxyadenosine 3′-monophosphate; SD, standard deviation.

10.1021/bi802122k CCC: $40.75
Published on Web 02/25/2009

"A" is thought to activate the 3′-ribosyl hydroxyl group for nucleophilic attack on the oxygen of the α-phosphate whereas the metal ion in site "B" coordinates with β- and γ-phosphates of ATP (*4, 5*). The ATP phosphates are themselves recognized by a phosphate-binding loop at the junction of the C1 domain β1-α1 element. Kinetic analysis shows that cAMP is released from the enzyme more rapidly than the second product, pyrophosphate (PP_i) (*28*). The enzyme adopts the open state upon product release, but it is not known whether the transition to this state occurs upon cAMP formation or release of cAMP or PP_i from the enzyme.

Previous studies have shown that Ca^{2+} inhibits AC5 and AC6 by a mechanism that is largely noncompetitive with respect to ATP (*9*). Calcium ion antagonizes the activation of these enzymes by Mg^{2+}, and this inhibition is biphasic with respect to Ca^{2+} concentration (*9, 25, 29*). Kinetic analysis of AC5 shows that, at submicromolar concentration, Ca^{2+} is a noncompetitive inhibitor of Mg^{2+} activation, and, at supramicromolar concentration, Ca^{2+} inhibition is directly competitive with Mg^{2+} (*25*). The interdependence of Mg^{2+} activation and Ca^{2+} inhibition in site-directed mutants of AC5 suggests that inhibition of AC by Ca^{2+} involves the Mg^{2+}-binding loci at the AC catalytic site. Indeed, mutations distal to the Mg^{2+} coordination site that affected Mg^{2+} binding also displayed impaired or diminished Ca^{2+} inhibition in direct proportion to diminution of activation by Mg^{2+} (*25*). That high-affinity Ca^{2+} binding is noncompetitive with respect to Mg^{2+} is suggestive of an allosteric mode of action, wherein Ca^{2+} modulates the conformational equilibrium of the enzyme. However, the mechanisms by which Ca^{2+} regulates AC remain to be understood at the molecular level.

Here, we present structural data that provides insight into the molecular mechanism by which Ca^{2+} inhibits AC5. Ideally, such an investigation would focus on the AC5 holoenzyme, or its catalytic domain, which is subject to the same mechanism of Ca^{2+} inhibition (*25*). However, biochemical studies have demonstrated that the catalytic and many of the regulatory properties of holo-AC are faithfully recapitulated by the Gαs-activated soluble VC1:IIC2 catalytic core of AC, which is amenable to crystallization (*30, 31*). Experiments conducted with chimeric AC molecules demonstrate that isoform-specific high-affinity inhibition by Ca^{2+} is conferred by the C1 domain but not the C2 domain of AC. Chimeric AC molecules composed of the transmembrane 1 (TM1) and C1 domains of AC5 and the TM2 and C2 domains of AC2 retain susceptibility to inhibition by submicromolar Ca^{2+}. In contrast, the corresponding constructs in which TM1/C1 is derived from AC2 and TM2/C2 from AC5 are not inhibited. High-affinity Ca^{2+} inhibition was also observed in experiments in which half-molecules composed of the TM and C1a (CHD only) domain of AC5 and the TM and C2 domain of AC2 were coexpressed (*25*). These experiments, together with evidence that Ca^{2+} acts at the Mg^{2+} cofactor binding sites, have prompted us to use Gαs·GTPγS:VC1:IIC2 as a model system to investigate the structural mechanism for high-affinity inhibition of AC5 by Ca^{2+}.

Here, we present kinetic evidence to demonstrate that, in the presence of Gαs·GTPγS and FSK, Ca^{2+} shows the same pattern of high- and low-affinity inhibition toward VC1:IIC2 that has been observed for holo AC5. We have determined a series of crystal structures of Gαs·GTPγS and FSK-activated VC1:IIC2 in the presence of Ca^{2+} that provide direct insight into the mechanism of Ca^{2+} inhibition. These structures were determined (1) in the presence of nonreactive ATP analogue and free Ca^{2+} at a concentration below the EC_{50} for high-affinity inhibition, (2) in the presence of ATP and free Ca^{2+} in the millimolar range sufficient to saturate both high- and low-affinity sites, and (3) in the presence of pyrophosphate and saturating Ca^{2+}. In conjunction with the latter, we have also determined the structure of the Gαs·GTPγS and FSK-activated AC catalytic core bound to the cofactor Mg^{2+} and pyrophosphate, the binary product complex. Together, these structures elucidate the mode of Ca^{2+} binding in the high- and low-concentration regimes and show that Ca^{2+} stabilizes the inactive (open) state of the enzyme in both ATP- and PP_i-bound states. Further, the structure of the PP_i-bound AC catalytic core provides insight into the nature of conformational changes that accompany the product-release phase of the AC catalytic cycle.

MATERIALS AND METHODS

Preparation of Protein Complexes. Recombinant mammalian adenylyl cyclase cytosolic VC1 and IIC2 domains and bovine Gαs proteins were expressed and purified as described (*32*). Before complex formation, the Gαs protein was activated by GTPγS and then trypsin-digested. A mixture of individually purified recombinant VC1, IIC2, and trypsin-treated Gαs·GTPγS was passed through sizing columns in the presence of excess MP-FSK and GTPγS. Fractions containing the heterotrimeric complex were identified by gel electrophoresis on a 4−20% Tris-HCl polyacrylamide gel (Bio-Rad, Hercules, CA). Fractions containing the complex were collected and concentrated to ~8 mg/mL in a buffer containing 20 mM Na^+HEPES (pH 8.0), 2 mM EDTA, 2 mM $MgCl_2$, 2 mM DTT, 100 mM NaCl, 25 μM MP-FSK, and 10 μM GTPγS for crystallization.

Crystallization, Structure Determination, and Model Refinement of the MP-FSK,Gαs·GTPγS:VC1:IIC2 Complex with Substrates and Ca^{2+} or Mg^{2+}. Crystals of the protein complex were grown, harvested, and cryoprotected as described previously (*32, 33*). Before cryoprotection, crystals were soaked in one of following reservoir solutions, 2 mM ATPαS and 50 μM $CaCl_2$ (for which the free [Ca^{2+}] was found to be 8 μM using the dye calibration method of Linse (*34*)), 5 mM ATP and 1.5 mM $CaCl_2$, 3 mM PP_i and 10 mM $MgCl_2$, or 3 mM PP_i and 2 mM $CaCl_2$ for 1−2 h at room temperature and then harvested in cryoprotectant solution containing the same concentrations of the respective ligands and metal ions. For crystallization of mAC at low [Ca^{2+}], crystals were soaked in reservoir solution containing 2 mM ATPαS and 50 μM $CaCl_2$, which were likewise present at the same concentrations in cryoprotectant solutions. Diffraction data sets were collected by the oscillation method at the Advanced Photon Synchrotron SBC-CAT ID-19 beamline or the Stanford Synchrotron Radiation Laboratory 9-1 beamline with an incident beam wavelength of 1.0454 or 1.0231 Å, respectively. Image processing and data reduction utilized the HKL2000 package (*35*). Due to anisotropy, data with *l* index >20 for crystals of the Gαs·GTPγS and FSK-activated VC1:IIC2 complexes with PP_i·Mg^{2+}, PP_i·Ca^{2+}, ATPαS·Ca^{2+}, or ATP·$2Ca^{2+}$ were excluded from the

Table 1: Summary of Data Collection and Refinement Statistics

parameter	AC·ATP·2Ca^{2+}	AC·ATPαS·Ca^{2+}	AC·PP_i·Ca^{2+}	AC·PP_i·Mg^{2+}
cell constants				
a (Å)	118.3	118.7	117.9	117.5
b (Å)	133.5	133.7	133.0	133.1
c (Å)	70.7	71.0	70.0	70.1
d_{min} (Å)	2.9	3.0	2.7	2.8
av redundancy	2.5 (2.1)	2.8 (2.1)	5.2 (3.0)[a]	3.1 (2.4)
R_{sym}[b] (%)	17.6 (55.2)	17.5 (41.4)	12.5 (33.4)	13.9 (43.5)
completeness (%)	91.7 (87.6)	82.7 (67.5)	95.9 (89.7)	91.7 (86.4)
$\langle I \rangle / \langle \sigma \rangle$	6.5 (1.2)	5.1 (1.6)	9.9 (2.2)	7.2 (1.8)
resolution range for refinement[c] (Å)	15−2.9	15−3.0	15−2.7	15−2.8
total reflections used	21380	18290	28220	23685
no. of protein atoms	5637	5627	5638	5691
no. of water molecules	6	12	33	12
no. of heterogen atoms	94	106	73	73
rmsd bond length (Å)	0.008	0.012	0.007	0.008
rmsd bond angle (deg)	1.100	1.453	1.102	1.128
R_{work}[d] (%)	24.9	23.9	24.5	23.7
R_{free}[e] (%)	29.9	30.9	29.1	29.2
ave overall B-factor (Å^2)	40.6	31.8	51.2	54.1
ave *B*-factor on substrate (Å^2)	52.1	85.0	67.8	71.4
ave *B*-factor on metal ion(s) (Å^2)	43.9	66.7	63.6	67.5
Ramachandran plot (%)				
favorable and allowed region	100	99.7	99.5	99.8
generously allowed region	0	0.3	0.5	0.2

[a] Numbers in parentheses refer to data in the highest resolution shell. [b] $R_{sym} = \sum_h \sum_i |I(h) - I(h)_i| / \sum_h \sum_i I(h)_i$, where $I(h)$ is the mean intensity after rejections. [c] Due to anisotropy, data with l index greater than 20 were omitted from refinement. [d] $R_{work} = \sum_h ||F_o(h)| - |F_c(h)|| / \sum_h |F_o(h)|$, where $F_o(h)$ and $F_c(h)$ are observed and computed structure factors; no I/σ cutoff was used during refinement. [e] 5% of the complete data set was excluded from refinement to calculate R_{free}.

data set used for refinement. The atomic coordinates from the isomorphous crystals of the MP-FSK,Gαs·GTPγS:VC1:IIC2 complex (PDB ID 1AZS) were used to compute initial phases for all four complexes (*27*). Atomic positions and thermal parameters were refined by successive rounds of rigid body refinement, simulated annealing, Powell minimization, and *B*-factor refinement using the CNS 1.1 program suite (*36*) or REFMAC5 (*37*) as implemented in the CCP4 program suite (*38*). Ligands and metal ion(s) were located in SIGMA-A weighted (*39*) difference omit maps computed with phases from refined models. Atomic models were iteratively improved by manual refitting into weighted $2|F_o| - |F_c|$ maps using the computer graphics model building programs O and Coot (*40, 41*) and subsequent cycles of refinement using CNS or REFMAC5. Diffraction and refinement statistics are given in Table 1. Figures were generated using PyMOL (DeLano Scientific LLC, San Carlos, CA; http://www.pymol.org). Coordinates for the AC·PP_i·Ca^{2+}, AC·PP_i·Mg^{2+}, AC·ATP·2Ca^{2+}, and AC·ATPαS·Ca^{2+} complexes have been deposited in the Protein Data Bank with the codes 3C14, 3C15, 3C16, and 3E8A, respectively.

Measurement of Adenylyl Cyclase Activity. Adenylyl cyclase activity was determined as described previously (*42*−*44*) with some modifications. Briefly, for meaurement of Ca^{2+} inhibition of Mg^{2+}, FSK, Gαs·GTPγS activated VC1:IIC2, adenylyl cyclase activity of purified VC1 (50 nM) and IIC2 (250 nM) was measured in the presence of the following components: 12 mM phosphocreatine, 2.5 units of creatine phosphokinase, 0.1 mM cAMP, 0.1 mM ATP, 0.04 mM GTP, 0.5 mM phosphodiesterase inhibitor, isobutylmethylxanthine, 1.25 μCi of [α-^{32}P]ATP, 0.75 mM $MgCl_2$, 10 μM FSK, or 500 nM Gαs·GTPγS, as indicated. Free Ca^{2+} concentrations were established using an EGTA-buffering system as described previously (*45*) and the BAD4 computer program (*24*). The reaction mixture (final volume, 100 μL) was incubated at 30 °C for 20 min. Reactions were terminated with sodium lauryl sulfate (0.5%); [8-^{3}H]cAMP (∼6000 cpm) was added as a recovery marker, and the [^{32}P]cAMP formed was quantitated as described previously (*46*).

For PP_i or Ca^{2+}/PP_i inhibition experiments, the activity of purified VC1 (100 nM) and IIC2 (500 nM) was measured in a buffer of 25 mM Na^+Hepes (pH 8.0) containing 20 mM phosphor(enol)pyruvate, 0.1 mM GTP, 3 units of pyruvate kinase, 0.1 mM ATP, 0.1 mM cAMP, 0.3 mM $MgCl_2$, 1 μCi of [α-^{32}P]ATP, 1 μM Gαs·GTPγS, and 100 μM FSK, unless stated otherwise. Free Ca^{2+} concentrations were established and calibrated using an EGTA-buffering system as described previously (*34*). Following a 2 min preincubation at 37 °C, reactions were conducted for 15 min at 37 °C and were terminated by the addition of 20 μL of 2.2 N HCl containing [^{3}H]cAMP. Denatured protein was additionally heated to 95 °C for 4 min, cooled on ice, and finally sedimented by a 1 min centrifugation at 15000*g*. Reaction mixtures were applied onto disposable columns filled with 1.3 g of neutral alumina. cAMP was separated from [α-^{32}P]-ATP by elution of cAMP with 0.1 M ammonium acetate, pH 7.0. [^{32}P]cAMP and [^{3}H]cAMP were measured by liquid scintillation spectrometry where [^{3}H]cAMP was calculated for the efficiency of cAMP recovery of each tube. Nonlinear regression curves and kinetic parameters were obtained using SigmaPlot software (SYSTAT Software Inc., San Jose, CA). Adenylyl cyclase activity is expressed per weight of VC1, and data points are presented as mean activities ± SD of triplicate determinations.

Measurement of ATP Synthesis. The measurement of ATP synthesis from cAMP and PP_i was performed as described previously (*28*) with some modifications. The reverse reaction of adenylyl cyclase was measured spectrophotometrically in the presence of the following components: 50 mM glucose, 20 mM Hepes, 1.2 units of hexokinase, 0.8 mM NADP, 2 mM $MgCl_2$, 2 mM PP_i, 0.5 units of glucose-6-phosphate

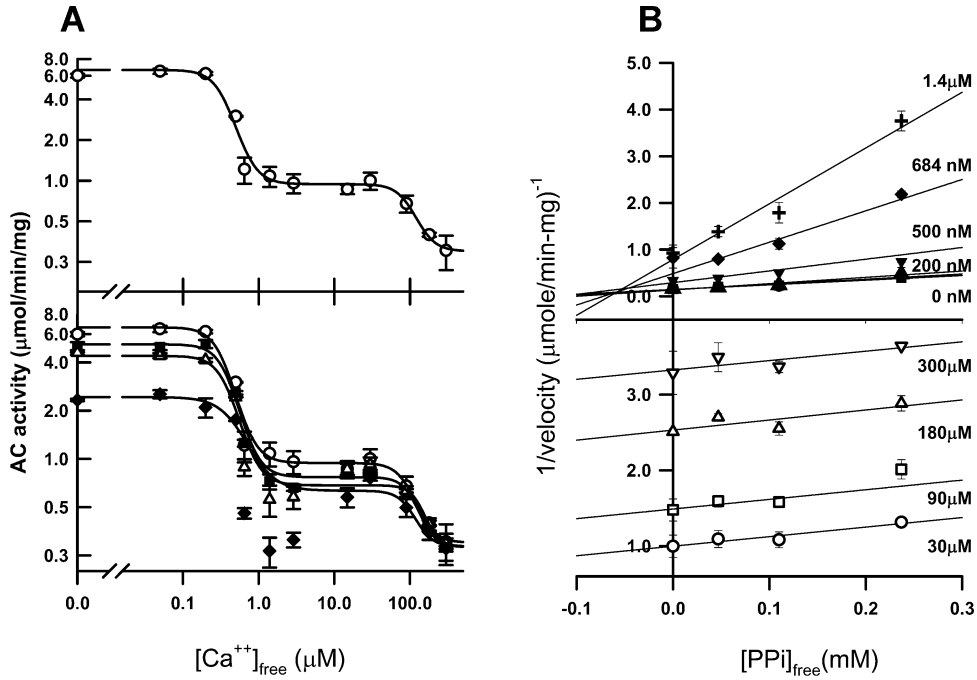

FIGURE 1: Biphasic inhibition of VC1:IIC2 activity in the presence and absence of pyrophosphate. (A) Activity of VC1 (50 nM) and IIC2 (250 nM) in the presence of 500 nM Gαs·GTPγS, and 10 μM FSK was determined in the absence (○; upper panel) or presence (lower panel) of a concentration of PP_i sufficient to inhibit AC activity by 25%, 50%, or 75% (47 μM (■), 115 μM (Δ), or 235 μM (◆), respectively). Data represent the mean ± SD of at least three independent experiments and were fit to a two-site competition model. (B) Dixon plot to show the relation between the submicromolar (upper panel) or supramicromolar concentration (lower panel) of Ca^{2+} and PP_i. The data were recast from the Ca^{2+} inhibition of AC activity that was determined in the absence or presence of a concentration of PP_i: ●, no added calcium; ▲, $[Ca^{2+}]_{free}$ = 200 nM; ▼, $[Ca^{2+}]_{free}$ = 500 nM; ◆, $[Ca^{2+}]_{free}$ = 684 nM; +, $[Ca^{2+}]_{free}$ = 1.40 μM; ○, $[Ca^{2+}]_{free}$ = 30 μM; □, $[Ca^{2+}]_{free}$ = 90 μM; Δ, $[Ca^{2+}]_{free}$ = 180 μM; ▽, $[Ca^{2+}]_{free}$ = 300 μM. For some data points, the width of the error bars is smaller than the symbol.

dehydrogenase, and the various concentrations of cAMP and $CaCl_2$. The reaction was started by the addition of 0.4 μM VC1, 2 μM IIC2, and 1 μM Gαs·GTPγS (final volume 400 μL, pH 7.4), incubated at 30 °C for 40 min. ATP synthesized was determined by the rate of NADP reduction as measured by the change in absorbance at 340 nm using an a Ultrospec 2100 Pro UV/visible spectrophotometer. A standard curve was obtained by measuring the rate of NADP reduction at a range of ATP concentrations in the absence of protein, cAMP, and PP_i. ATP synthesis activities were expressed per weight of VC1 and fitted with Lineweaver−Burk analysis using GraphPad Prism version 4. Data points were presented as mean activities ± SD of triplicate determinations.

Chemicals. GTPγS was obtained from Roche (Indianapolis, IN). FSK and MP-FSK were obtained from Merck (Nottingham, U.K.) or Calbiochem (La Jolla, CA). [α-^{32}P]-ATP (3000 Ci/mmol) was from Perkin-Elmer Life Sciences (Boston, MA) or GE Healthcare (Little Chalf-ont, U.K.). [8-^{3}H]cAMP was obtained from GE Healthcare (Little Chalf-ont, U.K.), and all other reagents were purchased from Sigma (Poole, U.K.).

RESULTS

Ca^{2+} Inhibition of Activated VC1:IIC2. As noted in the introduction, Ca^{2+} was shown to exert biphasic inhibition of AC5 and AC6 in cell lysates (*9, 25*). In the present work, we extended these studies to investigate Ca^{2+} inhibition of a purified soluble recombinant complex consisting of VC1 and IIC2. This complex possesses high catalytic activity upon activation by both FSK and Gsα·GTPγS protein (*31*), and thus experiments were conducted in the presence of 10 μM FSK and 500 nM Gαs·GTPγS. As is the case for holoenzyme preparations, inhibition of FSK and Gsα·GTPγS-activated VC1:IIC2 by Ca^{2+} is biphasic (Figure 1A), with EC_{50} values of 0.37 ± 0.03 and 100 ± 30 μM, respectively. The K_i of the high-affinity component is not significantly changed, whereas that of the low-affinity inhibition increased 2-fold over the range of $[Mg^{2+}]$ from 0.3 to 3 mM (data not shown). These results are comparable to data taken from cell lysates expressing AC5 where the range for high and low affinity of Ca^{2+} inhibition was 0.28 ± 0.21 and 32−163 μM, respectively (*25*), indicative of noncompetitive and competitive inhibition of Mg^{2+} activation of AC through the high- and low-affinity binding modes of Ca^{2+}.

Inhibition of VC1:IIC2 by PP_i and Ca^{2+}. AC activity in the direction of cAMP synthesis is inhibited by both reaction products, cAMP and PP_i (*28*). Product inhibition by PP_i has been shown to be noncompetitive with respect to ATP with an observed K_i of ∼300 μM. Over a range of PP_i concentrations, Ca^{2+} exhibits biphasic inhibition of VC1:IIC2 in the presence of Gαs·GTPγS and FSK (Figure 1A). A Dixon plot of 1/velocity versus the concentration of Ca^{2+} in the high-affinity range (200 nM−1.4 μM) intersects at a common point, consistent with nonexclusive inhibition by Ca^{2+} and PP_i of adenylyl cyclase (*47*) (Figure 1B, upper panel). The K_i of PP_i remains constant over this range of Ca^{2+}, indicating that the two inhibitors do not bind cooperatively. Values of reciprocal velocity at varying $[PP_i]$ at $[Ca^{2+}]$ in the low-affinity range (30−300 μM) give rise to a set of parallel lines, indicating that PP_i and Ca^{2+}, acting at a low-affinity site, are exclusive inhibitors (Figure 1B, lower panel). These kinetic data can be rationalized by the crystal structures of

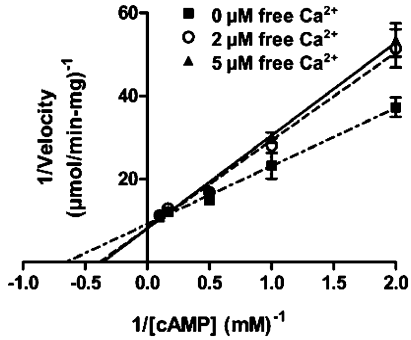

FIGURE 2: Ca^{2+} inhibition of ATP synthesis. Double reciprocal plots for inhibition by Ca^{2+} of ATP synthesis by VC1 (0.4 μM), IIC2 (2 μM), and 1 μM Gαs·GTPγS. Reactions were conducted in the absence (■) of Ca^{2+} or in the presence of 2 μM (○) or 5 μM (▲) free Ca^{2+}.

Ca^{2+} complexes with VC1:IIC2 described below. The origin of the sharp rise in AC activity in the 2.5−5 μM Ca^{2+} range, observed in the presence of PP_i, is not apparent. It is possible that, in this narrow concentration range, Ca^{2+} potentiation of ATP binding offsets the combined inhibitory effects of Ca^{2+} and PP_i on catalytic activity.

Effect of Ca^{2+} Inhibition on ATP Synthesis. To determine whether Ca^{2+} is an inhibitor of AC in the direction of ATP synthesis, we measured the rate of ATP production from cAMP and PP_i in the presence of Mg^{2+} at various Ca^{2+} concentrations. The reverse reaction, like the forward reaction, is also activated by Gsα·GTP and FSK, but with less potency (*28*). Double reciprocal plot analysis shows that Ca^{2+} causes a slight increase in the K_m for cAMP and no significant change in V_{max}. However, the inhibitory potency of Ca^{2+} reaches a plateau in the 2−5 μM range. Thus, Ca^{2+} appears to be a competitive partial inhibitor with respect to cAMP in the direction of ATP synthesis (Figure 2) with an inhibition constant similar to that for "high-affinity" inhibition of cAMP synthesis.

Crystal Structure of the VC1:IIC2 Complex with Ca^{2+} and ATPαS or ATP. We determined the structure of the Gαs·GTPγS/FSK-bound VC1:IIC2·ATPαS-R_p complex from crystals soaked in reservoir solution containing 8 μM free Ca^{2+}, well below the K_i for low-affinity Ca^{2+} inhibition. The isosteric and nonreactive ATP analogue ATPαS-R_p was used in this instance because VC1:IIC2 retains appreciable catalytic activity in the presence of micromolar Ca^{2+}. The structure of the VC1:IIC2·ATP complex was also determined from crystals containing 1.5 mM Ca^{2+}, sufficient to achieve maximal inhibition. The structures of the two complexes were determined at 3.0 Å (ATPαS-R_p) and 2.9 Å (ATP) resolution (Table 1) and are isomorphous with previously reported Gαs·GTPγS/FSK-bound VC1:IIC2 structures (*27*). Both the Ca^{2+}-bound ATP and ATPαS-R_p complexes adopt the "open" conformation characteristic of apo-VC1:IIC2 (Figure 3A), in contrast to the "closed" state seen in the complex of ATPαS-R_p with Mg^{2+} and Mn^{2+} (*5*). In the open state, the enzyme is not able to form the full complement of protein−nucleotide interactions that are possible for the closed state. Although VC1:IIC2 adopts an open conformation in both complexes, the mode of nucleotide−Ca^{2+} binding in the "low-Ca^{2+}" ATPαS-R_p complex differs significantly from that in the "high-Ca^{2+}" complex with ATP. The enzyme active site of the latter adopts a more open

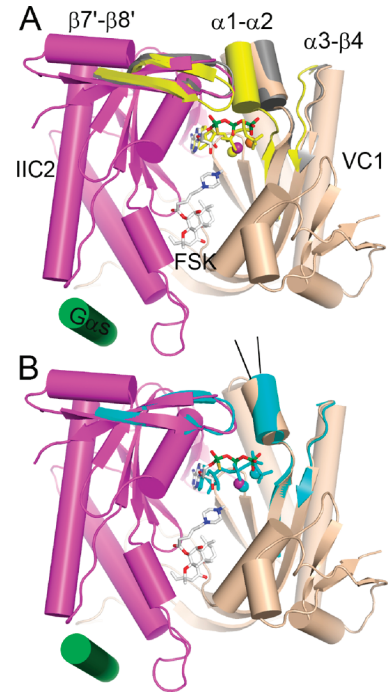

FIGURE 3: Global views of Gαs·GTPγS/FSK-activated VC1:IIC2 substrate complexes with Ca^{2+} or Mg^{2+}. (A) The structures of VC1 and IIC2 domains in the ATPγS·Ca^{2+} complex are shown in mauve and tan, respectively (*26*). Shown in superposition are the secondary structure elements β1-α1-α2 and α3-β4 of VC1 and β7′-β8′ of IIC2 in the open state VC1:IIC2 apoenzyme (PDB ID 1AZS), gray, and those of the closed state ATPαS complex with Mn^{2+} and Mg^{2+} (PDB ID 1CJK), yellow (*26, 27*). The switch II helix of the GTPγS-activated Gαs subunit is shown as a green cylinder. Ligands are drawn as stick models; for ATPαS and FSK, carbon atoms are in gray, nitrogens blue, oxygens red, and phosphorus green. Metal ions are shown as metallic spheres; Ca^{2+} ion is in violet, Mg^{2+} light yellow, and Mn^{2+} orange. This coloring scheme for atoms is retained in all figures unless otherwise noted. (B) Superposition of the secondary structure elements β1-α1-α2 and α3-β4 of VC1 and β7′-β8′ of IIC2 of the ATP·2Ca complex with two Ca^{2+} ions, cyan, with the VC1 and IIC2 domain structure of ATPαS·Ca, using the atomic coloring scheme as in panel A. The two structures are similar to each other except that the α1 helix of the ATPaS·Ca complex is rotated ~10° toward the IIC2 domain relative to the α1 helix of the ATP·2Ca complex (as shown by the lines indicating the α1 helix axis in two structures).

conformation due to a rotation of the C1 domain α1 helix away from the subunit interface (Figure 3B).

The $|F_o| - |F_c|$ difference electron density map for the ATPαS-R_p complex reveals continuous density for ATPαS-R_p and a single diffuse peak which we attribute to a Ca^{2+} ion (Figure 4A). This assignment is confirmed by the presence of positive difference density observed upon modeling a water molecule at that site (Figure 4B). Magnesium ion, which could be expected to bind in similar fashion, was not present in the soaking solution. We refer to this structure as the ATPαS·Ca^{2+} complex.

The nucleotide in the ATPαS·Ca^{2+} complex adopts a compact, arched conformation. The electron density, together with stereochemical constraints imposed during refinement, dictates a *gauche* conformation for the C(4′)−C(5′) ribosyl bond and a glycosyl bond angle in the mid-*anti* range, which together cause the α-thiophosphate to project away from the metal center. This mode of ATPαS-R_p binding contrasts with that in the "closed" complex with Mg^{2+} and Mn^{2+} bound to the metal A and B sites, respectively (*5*) (Figure 5A,B). The

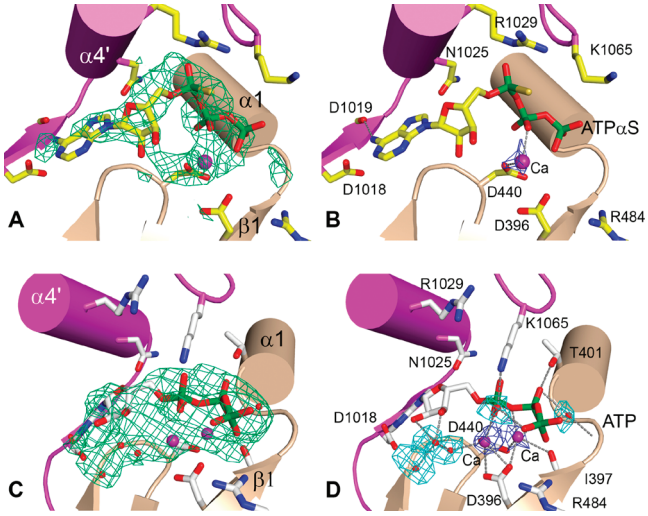

FIGURE 4: Binding of ATP and the inhibitor ATPαS to AC in the presence of high (1.5 mM) or low (8 μM) Ca^{2+}. Gαs·GTPγS/FSK-activated VC1:IIC2 bound to (A) ATPαS and Ca^{2+} or (C) ATP and two Ca^{2+} ions. The nucleotide, Ca^{2+} ions, and water molecules are shown as stick models or spheres. The 3.0 or 2.9 Å $|F_o| - |F_c|$ electron density maps, computed from the refined model from which coordinates for the Ca^{2+} and nucleotide in the ATPαs·Ca or ATP·2Ca complexes, respectively, are omitted and contoured at the 2.5σ level, is shown as lime green wire cages. Side chains of protein residues in the catalytic site are shown as sticks. The network of nonbonded interactions among (B) ATPαs and Ca^{2+} or (D) ATP, the two Ca^{2+} ions, water molecules, and side chains of protein residues is shown. Individual calcium ion(s) and water molecules are positioned according to the $|F_o| - |F_c|$ difference electron density maps calculated with the respective atoms omitted from the phasing model or Ca replaced with water. The difference maps for Ca^{2+} ion(s) and waters are contoured at the 3.0σ and 2.5σ level and shown as blue and cyan wire cages, respectively. The gray dashed lines depict hydrogen bonds (<3.2 Å) and metal coordination contacts (<3.0 Å) between ligand atoms, metal ions, water molecules, and protein residues. The hydrogen bonds, metal coordination contacts, single letter amino acid code, and residue ID numbers are shown for active site residues in this figure and in Figures 5 and 6.

purine ring of ATPαS-R_p in the Ca^{2+} complex is within hydrogen-bonding distance of the carbonyl oxygen atom of Ile-1019, affording interactions that provide specificity for adenine in preference to other nucleotide bases (*26, 48, 49*). However, as a consequence of the compact configuration of the nucleotide, and the open conformation of VC1:IIC2, the β- and γ-phosphate moieties cannot form hydrogen bonds with main-chain amides in the β1-α1 loop of VC1 (Figure 5B). The diffuse electron density for these phosphate moieties is indicative of a flexible binding mode.

The single Ca^{2+} ion observed in the ATPαS·Ca^{2+} complex occupies a position intermediate between the Mg^{2+} A and B sites (Figure 5B), although it is coordinated by the β- and γ-phosphates and both Asp-396 and Asp-440 as is typical for B site metal interactions (*5*). As noted above, the α-thiophosphate is not within coordination distance of the calcium ion. Electron density extending from the ribosyl group to the Ca^{2+} can be modeled as a water molecule bridging the ribose O(3′) and the calcium ion (Figure 4A). Even at the modest resolution of the structure, it is apparent that Ca^{2+}−oxygen ligand distances are longer than typically observed in protein−Ca^{2+} complexes, indicating that the metal is not rigidly coordinated (*50*).

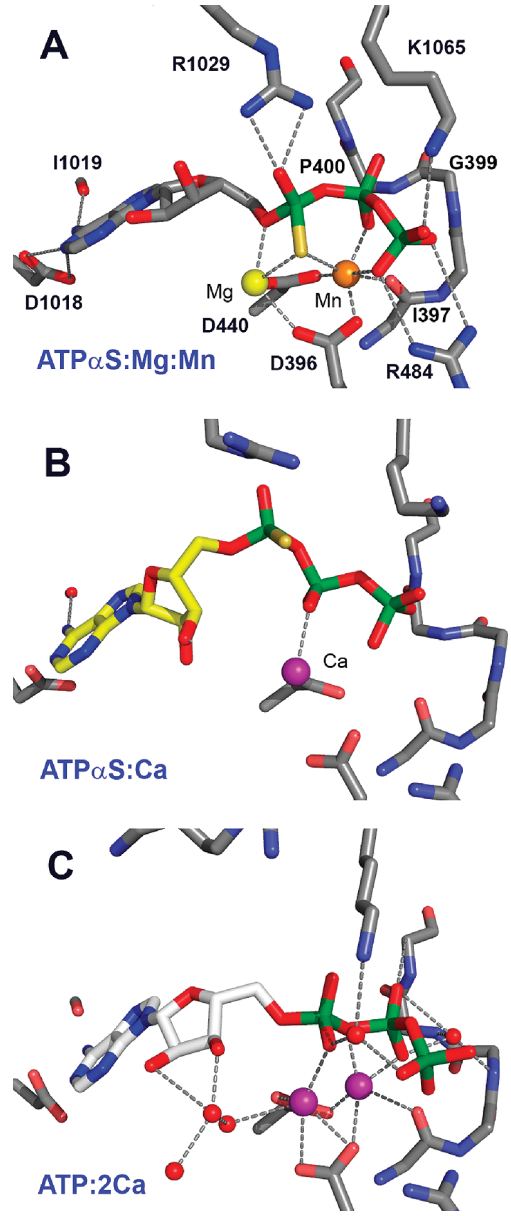

FIGURE 5: ATP or ATPαS coordination with Mg^{2+} or Ca^{2+} in the catalytic site of VC1:IIC2. (A) ATPαS:Mg^{2+}/Mn^{2+} (PDB ID 1CJK); (B) ATPαS·Ca; (C) ATP·2Ca. The main chain of the phosphate-binding loop (Ile-397-Thr-401 of VC1) and the side chains of substrate and metal ion interacting residues are shown and colored according to the scheme in Figure 4, except that carbon atoms are in gray, yellow, and white for ATPαS with Mg^{2+}, ATPαS with Ca^{2+}, and ATP, respectively.

The crystal structure of Gαs·GTPγS/FSK-activated VC1:IIC2 bound to ATP in the presence of millimolar Ca^{2+} exhibits two Ca^{2+} ions at the metal-binding site (Figure 4C). An $|F_o| - |F_c|$ electron density map computed with refined coordinates of the protein and bound nucleotide shows difference density at both Ca^{2+} sites, as well as weaker density that we attribute to ordered water molecules (Figure 4D). Accordingly, we refer to this structure as the ATP·$2Ca^{2+}$ complex. The metal ions are separated by only 3 Å, well under the separation distance expected for adjacent calcium ions. It is possible that the observed distance is an artifact of static disorder, as discussed below. The nucleotide triphosphate exhibits an extended conformation similar to that of ATPαS-R_p in the closed complex with Mg^{2+} and Mn^{2+} but is translated about 1 Å toward the β1-α1 relative

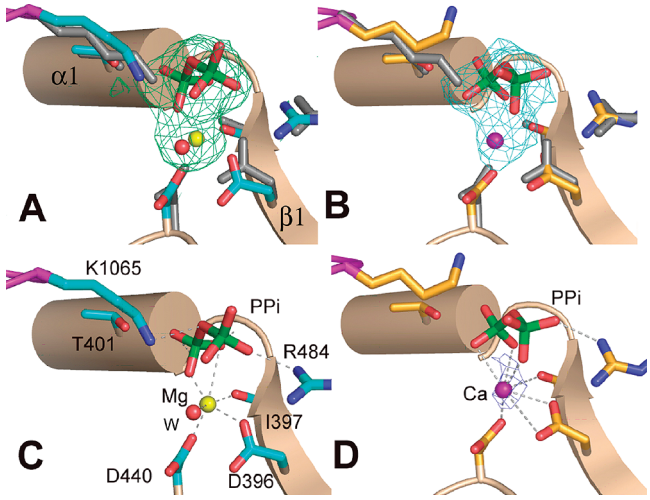

FIGURE 6: VC1:IIC2 complexes with $PP_i \cdot Ca^{2+}$ and $PP_i \cdot Mg^{2+}$. Electron density $|F_o| - |F_c|$ omit maps are shown as lime green wire cages that were calculated at the respective final resolution and contoured at the 2.5σ level for (A) the $PP_i \cdot Mg^{2+}$ and (B) the $PP_i \cdot Ca^{2+}$ complex. Models of PP_i with Mg^{2+} or Ca^{2+} at the B site are shown as stick models and spheres. A water molecule is observed adjacent to the Mg^{2+} at the B site, but no significant electron density is observed at the metal A site in either structure. Stick models of side chains of protein residues from the open conformation (1AZS) of VC1:IIC2 were superimposed onto both structures and depicted as gray-colored side chains. Interactions of $PP_i \cdot Mg^{2+}$ and $PP_i \cdot Ca^{2+}$ with the AC catalytic site residues are shown in panels C and D, respectively. The 2.8 or 2.7 Å $|F_o| - |F_c|$ electron density maps for the $PP_i \cdot Mg^{2+}$ or $PP_i \cdot Ca^{2+}$ complexes, respectively, are contoured at the 2.5σ level and shown as lime green wire cages. In panel D, the blue wire cage represents electron density contoured at 3.0σ for the 2.8 Å $|F_{o_{Ca}}| - |F_{o_{Mg}}|$ omit map, indicating that Ca^{2+} binds at site B. The VC1:IIC2 product complex with pyrophosphate and Mg^{2+} is, like that with Ca^{2+}, in the open conformation. Ligand and side chain atoms of protein residues are drawn as stick models with carbon atoms colored in cyan or orange for the $PP_i \cdot Mg^{2+}$ or $PP_i \cdot Ca^{2+}$ complexes, respectively.

to the latter (Figure 6A,C). This relative translation may be due to the expansion of the metal coordination sphere required to accommodate two calcium ions, which have larger radii (1.14 Å) than Mg^{2+} (0.86 Å) and Mn^{2+} (0.89 Å). The expansion of the coordination sphere forces the metal ligands in the β1-α1 loop (carboxylate of Asp-396 and carbonyl oxygen of Ile-397) away from the catalytic site, with the collateral loss of interactions between the ATP β- and γ-phosphates and the main-chain amides of Gly-399 and Phe-400 observed in the closed conformation of VC1:IIC2. Consequently, the CHD domains of $ATP \cdot 2Ca^{2+}$ adopt a somewhat more open conformation than that of $ATP\alpha S \cdot Ca^{2+}$, such that α1 helix is rotated about 10° further away from the C1:C2 interface (Figure 3B). Likewise, the adenosine moiety is not close enough to Asp-1018 and Ile-1019 to form hydrogen bonds or van der Waals contacts with these side chains in the base recognition pocket (Figure 6A,C). Further, the more open conformation at the C1:C2 domain interface does not allow for an ion pair interaction between Arg-1029 of the C2 domain with the α-phosphate oxygen atoms of ATP as observed in the $ATP\alpha S \cdot Mn^{2+} \cdot Mg^{2+}$ complex. This interaction has a key role in transition state stabilization (*27, 51, 52*).

Water-mediated interactions contribute to ATP binding in the open complex with Ca^{2+}. In the closed state, Lys-1065 of the C2 domain $\beta7'$-$\beta8'$ hairpin loop forms ionic contacts with α- and γ-phosphates of the nucleotide. In the $ATP \cdot 2Ca^{2+}$ complex, this ionic interaction is mediated by a water molecule (Figures 4C,D and 5C). A network of water molecules tethers ATP to Ca^{2+} and protein. The 3′-hydroxyl of the ribose forms water-mediated contacts with the A site Ca^{2+}. The triphosphate of ATP is also stabilized by a water molecule that coordinates with two oxygen atoms of the β- and γ-phosphates and two backbone amine groups of Gly-399 and Phe-400 (Figures 4D and 5C) at the N-terminus of the C1 domain α1 helix. These hydrogen bonds match those interactions between the β1-α1 loop and triphosphates of ATPαS in the closed state. Thus, $ATP \cdot 2Ca^{2+}$ is accommodated in the catalytic site despite the loss of direct interactions with the C2 domain while retaining contacts with the C1 domain. These observations are consistent with the evidence that the C1 domain mediates the effect of Ca^{2+} on the catalytic activity of AC (*25*).

The triphosphate moiety of ATP is fully engaged in coordination of the two Ca^{2+} ions in the $ATP \cdot 2Ca$ complex. The resolution of the structure does not permit accurate determination of Ca^{2+}−ligand coordination distances, yet the probable protein ligands can be identified. The equatorial plane of Ca^{2+} ligands comprises an α-phosphate oxygen, one or both carboxylate oxygen atoms of Asp-396, and a water molecule. On one face of the equatorial plane, an axial ligand is provided by a carboxylate oxygen of Asp-440, while the opposite face is empty, possibly occupied by a disordered water molecule. The A site Ca^{2+} is shifted about 2 Å closer to the Asp-396 carboxylate than the corresponding Mg^{2+} of the closed ATPαS complex and so is able to form more contacts with protein ligands than the latter. The B site Ca^{2+} is still more tightly bound with nearly hexadentate geometry. The equatorial plane is populated by one oxygen atom of Asp-440, a β-phosphate oxygen, the backbone carbonyl oxygen of Ile-397, and the ATP α,β-phosphate bridging oxygen. A carboxylate oxygen of Asp-396 and the ATP γ-phosphate contribute axial oxygen ligands. This mode of Ca^{2+} coordination is nearly identical to that observed for Mn^{2+} in the closed complex with ATPαS.

Structures of VC1:IIC2 Bound to Pyrophosphate and Ca^{2+} or Mg^{2+}. Crystals of VC1:IIC2 bound to PP_i in conjunction with either Ca^{2+} or Mg^{2+} diffracted to 2.7 and 2.8 Å resolution, respectively (Figure 6). These represent, to our knowledge, the first structures to be determined of a AC terminal product complex with pyrophosphate. Comparison with the unliganded enzyme shows that the β1-α1-α2 and α3-β4 loops of VC1 and $\beta7'$-$\beta8'$ of IIC2 in the $PP_i \cdot Ca^{2+}$- and $PP_i \cdot Mg^{2+}$-bound complexes conform to the open conformation of AC (Figure 3A). Global and local structural differences among apo VC1:IIC2 and the $PP_i \cdot Ca^{2+}$ and $PP_i \cdot Mg^{2+}$ complexes are minimal with root-mean-square deviations among equivalent Cα positions of 0.41−0.55 Å.

The electron density omit map for both the $PP_i \cdot Mg^{2+}$ and $PP_i \cdot Ca^{2+}$ complexes of VC1:IIC2 can be unambiguously fit to a model consisting of pyrophosphate bound to a magnesium ion with a water molecule or a single calcium cation, respectively (Figure 6A,B). Superposition of the $PP_i \cdot Ca^{2+}$-bound VC1:IIC2 complex with that of the enzyme bound to Mg^{2+}/Mn^{2+} and ATPαS confirms that the calcium ion binds to the metal B site in the pyrophosphate complex. Difference Fourier analysis of the diffraction data obtained from crystals soaked in $PP_i \cdot Ca^{2+}$ and $PP_i \cdot Mg^{2+}$ revealed strong $|F_{Ca}{}^{obs} -$

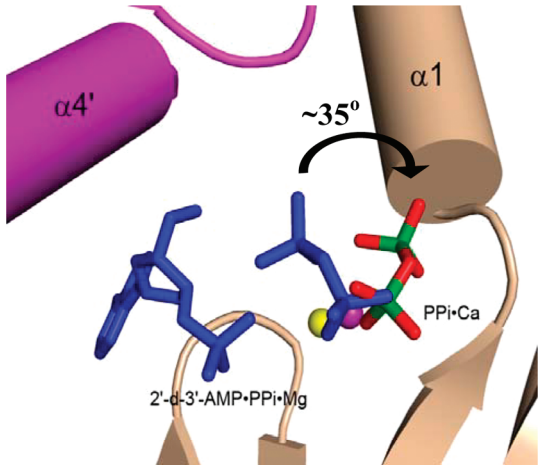

FIGURE 7: A detailed view of 2′-d-3′-AMP•PP_i•Mg^{2+} and PP_i•Ca^{2+} complexes in the catalytic site of the superimposed complexes. The PP_i is rotated ~35 °C toward to the β1-α1 loop of VC1 relative to the pyrophosphate moiety of the 2′-d-3′-AMP•PP_i•Mg^{2+} complex (PDB ID 1CS4). Calcium ion in the complex with PP_i occupies the B site as does Mg^{2+} in the complex with 2′-d-3′-AMP•PP_i (shown in blue).

F_{Mg}^{obs}| difference electron density at the metal "B" site (Figure 6D), confirming that the B site contains Ca^{2+} in the former complex. Neither the PP_i complex with Mg^{2+} nor that with Ca^{2+} shows electron density at the metal A site.

The orientation of pyrophosphate in the active site of the open state AC complexes described here differs from the β,γ-diphosphate moiety of ATPαS in the closed state complex with Mg^{2+} and Mn^{2+} (*5*) (Figure 4B) and from pyrophosphate in the closed complex with the P site analogue 2′-d-3′-AMP (*53*). Essentially, the Pβ−Pγ axis of the pyrophosphate rotates in conjunction with the change in the orientation of the C1 domain α1 helix in the transition from the closed to the open states of the enzyme. Consequently, hydrogen bond contact between the backbone amide groups of the α1 helix and PP_i is maintained in both open and closed conformations. In the open state complexes with Mg^{2+} or Ca^{2+}, the PP_i phosphate distal to the C1 domain α1 helix (Pγ) is located in approximately the same position as the γ-phosphate of the substrate analogue in the ATPαS complex (Figure 4B) and its counterpart in the 2′-d-3′-AMP•PP_i complex (*5*) (Figure 7). An oxygen atom from Pγ forms ion pair bonds with the positively charged guanidinium amides of Arg-484 from VC1 as seen in other structures of AC bound to substrate analogues, "P site" and fluorophore-substituted inhibitors (Figure 6C) (*5, 33, 53, 54*). The proximal phosphate (Pβ) is oriented toward the β1-α1 loop of VC1 and forms hydrogen bonds with the backbone amides of Gly-399 and Phe-400. This is in contrast to the closed complex with 2′-d-3′-AMP•PP_i, where the PP_i Pγ phosphate forms hydrogen bonds with the amide of Gly-399 and the proximal phosphate is hydrogen bonded to the amide groups of Phe-400 and Thr-401 (*53*). Thus, the Pβ−Pγ axis of the pyrophosphate, which is aligned with the peptide bonds of residues 399−401 in the closed P site complex, rotates ~35° in the PP_i•Ca^{2+}(Mg^{2+}) complexes. This rotation allows the Pγ moiety to maintain hydrogen bond contact with the α1 helix as it swings into the open state (Figure 7).

The amino acid side chains that interact with the metal ion and PP_i maintain similar conformations in the Ca^{2+} and Mg^{2+} complexes with two significant exceptions. First, Asp-396 adopts a different rotomeric state in the complex with Ca^{2+}, wherein both carboxylate oxygen atoms contact the metal ion, in comparison to the Mg^{2+} complex, in which only one of the carboxylate oxygen atoms is a metal ligand (Figure 6C,D). Second, Lys-1065 forms an ion pair with the bridging oxygen of PP_i in the PP_i•Mg^{2+} complex but not in the complex with Ca^{2+}. It appears that the loss of this ionic interaction is compensated by an additional coordinating contact between the Pβ phosphate and the metal ion. Interactions between Lys-1065 and phosphate groups of substrate analogues are generally observed in complexes with ATP analogues or fluorophore-substituted nucleotides, in which the enzyme adopts a closed or semiclosed conformation (*5, 54*).

B site Ca^{2+} coordination in the PP_i complex is heptadentate, with some differences in the atoms that form the coordination sphere. A carboxylate oxygen of Asp-396 and an oxygen atom of Pγ form axial ligands, and five equatorial ligands contributed by Asp-396, Asp-440, the carbonyl of Ile-397, and Pβ form a rough pentagonal array. B site Mg^{2+}coordination in the PP_i•Mg^{2+} complex is, in contrast, octahedral, involving oxygen ligands from Pβ, three VC1 residues (Asp-396, Asp-440, and Ile-397), and a water molecule (Figure 6C) but no interaction with Pγ. The mode of PP_i −metal coordination observed here differs from that in the closed complex with 2′-d-3′-AMP•PP_i•Mg^{2+}, a mimic of the cAMP•PP_i complex, where the 3′ nucleotide phosphate serves as the axial ligand of the B site metal in place of a water molecule (*53*). In the closed complex with ATPαS, the α-thiophosphate acts in a similar role (Figure 5A). In both of the latter complexes the Pγ of PP_i, or the corresponding nucleotide γ-phosphate, participates in metal coordination.

DISCUSSION

The data presented here provide strong evidence that Ca^{2+} inhibits AC5 by displacing the Mg^{2+} cofactors at the catalytic site. Accordingly, mutations of residues adjacent to (Cys-441 or Tyr-442) or remote from (Phe-423 and Arg-434) the Mg^{2+} binding site that diminish sensitivity of AC5 to inhibition by Ca^{2+} also impair enzyme activation by Mg^{2+} (*25*). Further, Ca^{2+} stabilizes an open, catalytically inactive conformation of the C1 and C2 domains of AC. This is the case for both the substrate complex with ATP and pyrophosphate product complex. Because AC assumes an open conformation in the PP_i-bound state, Ca^{2+} inhibits AC by stabilizing the enzyme−product complex.

The biphasic inhibition of AC5 by Ca^{2+} is recapitulated in the hybrid catalytic core composed of VC1 and IIC2. Inhibition by Ca^{2+} at micromolar concentration, a hallmark of AC5 and AC6, arises from binding at a location close to the A site. However, coordination of the metal is B site-like, such that Ca^{2+} is loosely bound in an electronegative cage formed by the β- and γ-phosphates of ATP and by Asp-396 and Asp-440. In this complex the substrate analogue ATPαS adopts an arched conformation that does not permit interaction of its α-phosphate with either Ca^{2+} or with residues, such as Arg-1029, that provide transition state stabilization (Figure 5B) (*27*). The compact conformation of the nucleotide is unlikely to be due to the presence of the R_p thiolate at the α-phosphate since ATPαS adopts an extended conformation in the closed state complex with Mg^{2+} and Mn^{2+} (Figure 5A) (*5*).

The noncompetitive relationship reported earlier between Mg^{2+} activation and high-affinity Ca^{2+} inhibition (*9*) arises in part from stabilization, by Ca^{2+}, of an open conformation of the ATPαS·Ca complex. Further, because the nucleotide β- and γ-phosphates are engaged in binding Ca^{2+} near the A site, they are unavailable for Mg^{2+} binding at site B. A conformational transition, similar to that which occurs upon binding a second calcium ion (see below), could accommodate Mg^{2+} at the B site, leaving Ca^{2+} bound to site A. However, unlike Mg^{2+}, a calcium ion would not activate the O-3′ hydroxyl of ATP for nucleophilic attack upon the α-phosphate. Thus, A site Ca^{2+} binding is inhibitory.

At ~100 μM concentration, Ca^{2+} binds to both A and B sites of open state VC1:IIC2. Because at that concentration a calcium ion is already bound to AC with B site-like coordination, it is likely that A site coordination is responsible for the low-affinity limb of the biphasic Ca^{2+} inhibition pattern. Binding of the second Ca^{2+} could be accompanied by translation of the first-bound Ca^{2+} to the B site locus. This is likely to occur in concert with the conformational transition of ATP to an extended conformation (Figure 6C) (Supporting Information movie). However, because the expanded Ca^{2+} coordination sphere does not permit direct interactions between the β and γ ATP phosphate with the β1-α1 loop, AC remains in the open conformation. Rather, these phosphate moieties form water-mediated interactions with the amide groups in the open form of that loop. Bound to the open conformation of AC, ATP is misaligned with the catalytic residues. Interaction of Arg-1029 with the α-phosphate of ATP, which provides transition state stabilization, and hydrogen bonding of Asn-1025 to the ribose endocyclic oxygen, which may be important for substrate orientation (*5*), do not occur in the Ca^{2+} Complex (Figure 4D). Nonproductive binding and the failure of Ca^{2+} to provide catalytic activation at the A site ensure that ATP does not turn over in crystals of Ca^{2+}-bound VC1:IIC2.

The distance between the two Ca^{2+} ions bound to the A and B sites of the ATP·2Ca complex is considerably less than that observed between adjacent divalent ions (Mg^{2+} or Mn^{2+}) that share coordinating ligands in other mAC complexes (*5*) or in RNA polymerase (*55*). The ionic radius of Ca^{2+} is larger than that of Mg^{2+} and Mn^{2+}, consistent with separations between adjacent calcium ions ranging from 3.8 to 4.3 Å in the 2.5 Å resolution structure of the C2 domain of protein kinase Cβ (*56*). It is possible that the more weakly bound site A Ca^{2+} is partially occupied, such that the B site Ca^{2+} comes to occupy an intermediate position in asymmetric units in which site A is unfilled. The Ca^{2+} positions reported here only represent average values for the two calcium ions in the refined structures. In fact, the distances between the two calcium ions range from 2.8 to 4.5 Å depending on the refinement constraints, consistent with dynamic interactions among two calcium ions, ATP, and neighboring protein residues and the modest resolution to which the crystals of the ATP·2Ca complex diffract.

Product release from AC does not follow an obligate ordered mechanism, but cAMP dissociates more rapidly than pyrophosphate from the catalytic site (*28*). The structural data reported here are consistent with the hypothesis that AC reverts to an open conformation upon release of cAMP, while pyrophosphate and Mg^{2+} are still bound to the enzyme. Mg^{2+} occupies the B site at this stage of the catalytic cycle and is tethered in an octahedral coordination sphere to oxygen atoms of the Pβ pyrophosphate phosphate and to the two conserved and catalytically essential aspartate residues at positions 396 and 440. Hence, in the absence of stabilizing interactions with the purine moiety of the adenine nucleotide, and of metal ion-mediated interactions that link the nucleotide monophosphate and pyrophosphate groups, AC reverts to the relaxed, open conformation. The structure of the PP_i·Mg^{2+} complex shows that PP_i is a noncompetitive inhibitor of AC because it stabilizes an open conformation of the enzyme to which ATP cannot bind productively.

High-affinity Ca^{2+} inhibition is nonexclusive with respect to pyrophosphate (Figure 1B) but appears to be exclusive at the low-affinity site. Even at millimolar concentration, only a single Ca^{2+} is bound to the VCI:IIC2·PP_i complex, where it occupies the Mg^{2+} B site and forms similar interactions with PP_i and the conserved aspartate residues. The exclusivity between inhibition by PP_i and by Ca^{2+} acting at the low-affinity site is probably due to the absence of the low-affinity A site in the open complex to which PP_i binds. The A site is formed in part by the α-phosphate of ATP, which has no analogue in the PP_i complex.

Ca^{2+} is a micromolar inhibitor of ATP synthesis but is competitive with cAMP. However, since increase in Ca^{2+} from 2 to 5 μM is not accompanied by an appreciable decrease in AC activity, it is possible that Ca^{2+} supports catalytic activity, possibly through interaction at the B site. The mechanism of this interaction requires further study.

Most vertebrate adenylyl cyclases, AC2, AC4, and AC7, for example, are not inhibited by micromolar Ca^{2+}. Molecular modeling of the type II AC CHD domain onto the open conformation of the VC1:IIC2 structure (1AZS) reveals several nonconserved amino residues around the catalytic site. The insensitivity of type II AC to submicromolar Ca^{2+} might be attributed to local features of the binding site (see Supporting Information Figures S1 and S2). For example, substitution of Ala-409 of VC1 with Pro-307 of IIC1 might restrict the movement of α1-α2 helixes upon binding of Ca^{2+} to the B site.

In contrast to AC5, bicarbonate-activated soluble adenylyl cyclase (sAC) is stimulated by Ca^{2+}, which, with an EC_{50} ~750 μM, decreases the K_m of the enzyme for ATP from 10 to 1 mM (*57, 58*). Crystallographic studies of the homologous sAC from *Cyanobacteria* have revealed open and closed conformational states that approximate those observed in VC1:IIC2 (*59*). Structures of the cyanobacterial sAC catalytic core in complex with ATPαS or $AMP(CH)_2PP$ and Ca^{2+} (or Ca^{2+} mimetics Sr^{2+} and Eu^{3+}) reveal exclusive binding of Ca^{2+} at the B metal site that leaves the Mg^{2+} site unoccupied. The cyanobacterial sAC adopts an open conformation, particularly with respect to the β1-α1 element, that is similar to that of the Ca^{2+}-bound VC1:IIC2 complexes. However, ATP is tightly bound, with contacts to both nucleoside and phosphate moieties, in the open, Ca^{2+}-bound state of sAC. Thus, by stabilizing the nucleotide β- and γ-phosphates at the active site, the heptacoordinate Ca^{2+} increases affinity for nucleotide, without fully destabilizing the metal A site for Mg^{2+} binding. We propose that global features of the catalytic site in the basal states of class III ACs dictate their susceptibility to either activation or inhibition by Ca^{2+}. It is probable that these structural features, which determine the volume of the active site and disposition

of purine, metal ion, and phosphate-binding residues, are determined by many residues at and surrounding the interface between the CHD domains.

The mechanisms by which AC activity is dynamically regulated by Ca^{2+} are complex, involving differential responses by various AC isoforms, contingent on patterns of tissue-specific expression. The data presented here, in the context of previous studies, reveal the molecular mechanism by which fluctuations in the physiological concentration of Ca^{2+} might directly attenuate cAMP production by AC5 and AC6.

ACKNOWLEDGMENT

We thank the staffs at the Advanced Proton Synchrotron SBC-CAT ID-19 beamline and the Stanford Synchrotron Radiation Laboratory 9-1 beamline for assistance with data collection.

SUPPORTING INFORMATION AVAILABLE

A movie showing the model of conformational transition of ATP in the mAC catalytic core during calcium binding. First depicted is a model of the open conformation of mAC (based on PDB ID 1AZS) bound to ATP and two Mg^{2+} ions (yellow spheres). The enzyme morphs to a closed conformation, based on PDB ID 1CJK. The Mg^{2+} is replaced by Ca^{2+} (magenta sphere), which is shown to occupy the B site. The complex then morphs to that of the ATPαS·Ca^{2+} complex reported here (PDB ID 3E8A), in which Ca^{2+} is bound to the high-affinity site and AC transits to an open conformation. Addition of a second Ca^{2+} results in the transition of the nucleotide to an extended conformation. The catalytic Arg-1029 moves away from the ATP α-phosphate, with both A and B sites occupied by Ca^{2+} (PDB ID 3C16). Figure S1 shows the structure-based alignment of amino acid sequences of the type V and II mAC C1 domains. Figure S2 show the model of type II mAC CHD domains. This material is available free of charge via the Internet at http://pubs.acs.org.

REFERENCES

1. Sunahara, R. K., Dessauer, C. W., and Gilman, A. G. (1996) Complexity and diversity of mammalian adenylyl cyclases. *Annu. Rev. Pharmacol. Toxicol. 36*, 461–480.
2. Buck, J., Sinclair, M. L., Schapal, L., Cann, M. J., and Levin, L. R. (1999) Cytosolic adenylyl cyclase defines a unique signaling molecule in mammals. *Proc. Natl. Acad. Sci. U.S.A. 96*, 79–84.
3. Garbers, D. L., and Johnson, R. A. (1975) Metal and metal-ATP interactions with brain and cardiac adenylate cyclases. *J. Biol. Chem. 250*, 8449–8456.
4. Zimmermann, G., Zhou, D., and Taussig, R. (1998) Mutations uncover a role for two magnesium ions in the catalytic mechanism of adenylyl cyclase. *J. Biol. Chem. 273*, 19650–19655.
5. Tesmer, J. J. G., Sunahara, R. K., Johnson, R. A., Gilman, A. G., and Sprang, S. R. (1999) Two metal ion catalysis in adenylyl cyclase. *Science 285*, 756–760.
6. Krupinski, J., and Cali, J. J. (1998) Molecular diversity of the adenylyl cyclases. *Adv. Second Messenger Phosphoprotein Res. 32*, 53–79.
7. Hanoune, J., and Defer, N. (2001) Regulation and role of adenylyl cyclase isoforms. *Annu. Rev. Pharmacol. Toxicol. 41*, 145–174.
8. Cooper, D. M., Mons, N., and Karpen, J. W. (1995) Adenylyl cyclases and the interaction between calcium and cAMP signalling. *Nature 374*, 421–424.
9. Guillou, J. L., Nakata, H., and Cooper, D. M. (1999) Inhibition by calcium of mammalian adenylyl cyclases. *J. Biol. Chem. 274*, 35539–35545.
10. Squire, L. R., Bloom, F., McConnell, S. K., Roberts, J. L., Spitzer, N., and Zigmond, M. J. (2003) *Fundamental Neuroscience*, 2nd ed., Academic Press, San Diego.
11. Willoughby, D., and Cooper, D. M. (2007) Organization and Ca^{2+} regulation of adenylyl cyclases in cAMP microdomains. *Physiol. Rev. 87*, 965–1010.
12. Cooper, D. M. (2003) Molecular and cellular requirements for the regulation of adenylate cyclases by calcium. *Biochem. Soc. Trans. 31*, 912–915.
13. Cooper, D. M., Karpen, J. W., Fagan, K. A., and Mons, N. E. (1998) Ca(2+)-sensitive adenylyl cyclases. *Adv. Second Messenger Phosphoprotein Res. 32*, 23–51.
14. Fagan, K. A., Mons, N., and Cooper, D. M. (1998) Dependence of the Ca^{2+}-inhibitable adenylyl cyclase of C6-2B glioma cells on capacitative Ca^{2+} entry. *J. Biol. Chem. 273*, 9297–9305.
15. Tang, W.-J., Krupinski, J., and Gilman, A. G. (1991) Expression and characterization of calmodulin-activated (type I) adenylyl cyclase. *J. Biol. Chem. 266*, 8595–8603.
16. Xia, Z., and Storm, D. R. (1997) Calmodulin-regulated adenylyl cyclases and neuromodulation. *Curr. Opin. Neurobiol. 7*, 391–396.
17. Wu, Z. L., Thomas, S. A., Villacres, E. C., Xia, Z., Simmons, M. L., Chavkin, C., Palmiter, R. D., and Storm, D. R. (1995) Altered behavior and long-term potentiation in type I adenylyl cyclase mutant mice. *Proc. Natl. Acad. Sci. U.S.A. 92*, 220–224.
18. Wayman, G. A., Impey, S., and Storm, D. R. (1995) Ca^{2+} inhibition of type III adenylyl cyclase in vivo. *J. Biol. Chem. 270*, 21480–21486.
19. Choi, E. J., Xia, Z., and Storm, D. R. (1992) Stimulation of the type III olfactory adenylyl cyclase by calcium and calmodulin. *Biochemistry 31*, 6492–6498.
20. Paterson, J. M., Smith, S. M., Simpson, J., Grace, O. C., Sosunov, A. A., Bell, J. E., and Antoni, F. A. (2000) Characterisation of human adenylyl cyclase IX reveals inhibition by Ca(2+)/Calcineurin and differential mRNA plyadenylation. *J. Neurochem. 75*, 1358–1367.
21. Brostrom, M. A., Brotman, L. A., and Brostrom, C. O. (1982) Calcium-dependent adenylate cyclase of pituitary tumor cells. *Biochim. Biophys. Acta 721*, 227–235.
22. Caldwell, K. K., Boyajian, C. L., and Cooper, D. M. (1992) The effects of Ca^{2+} and calmodulin on adenylyl cyclase activity in plasma membranes derived from neural and non-neural cells. *Cell Calcium 13*, 107–121.
23. Colvin, R. A., Oibo, J. A., and Allen, R. A. (1991) Calcium inhibition of cardiac adenylyl cyclase. Evidence for two distinct sites of inhibition. *Cell Calcium 12*, 19–27.
24. Gu, C., and Cooper, D. M. (2000) Ca(2+), Sr(2+), and Ba(2+) identify distinct regulatory sites on adenylyl cyclase (AC) types VI and VIII and consolidate the apposition of capacitative cation entry channels and Ca(2+)-sensitive ACs. *J. Biol. Chem. 275*, 6980–6986.
25. Hu, B., Nakata, H., Gu, C., De Beer, T., and Cooper, D. M. (2002) A critical interplay between Ca^{2+} inhibition and activation by Mg^{2+} of AC5 revealed by mutants and chimeric constructs. *J. Biol. Chem. 277*, 33139–33147.
26. Sinha, S. C., and Sprang, S. R. (2007) Structures, mechanism, regulation and evolution of class III nucleotidyl cyclases. *Rev. Physiol. Biochem. Pharmacol. 160*, 105–140.
27. Tesmer, J. J. G., Sunahara, R. K., Gilman, A. G., and Sprang, S. R. (1997) Crystal structure of the catalytic domains of adenylyl cyclase in a complex with $G_{s\alpha}$·GTPγS. *Science 278*, 1907–1916.
28. Dessauer, C. W., and Gilman, A. G. (1997) The catalytic mechanism of mammalian adenylyl cyclase. Equilibrium binding and kinetic analysis of P-site inhibition. *J. Biol. Chem. 272*, 27787–27795.
29. Yoshimura, M., and Cooper, D. M. (1992) Cloning and expression of a Ca(2+)-inhibitable adenylyl cyclase from NCB-20 cells. *Proc. Natl. Acad. Sci. U.S.A. 89*, 6716–6720.
30. Whisnant, R. E., Gilman, A. G., and Dessauer, C. W. (1996) Interaction of the two cytosolic domains of mammalian adenylyl cyclase. *Proc. Natl. Acad. Sci. U.S.A. 93*, 6621–6625.
31. Sunahara, R. K., Dessauer, C. W., Whisnant, R. E., Kleuss, C., and Gilman, A. G. (1997) Interaction of G_{sa} with the cytosolic domains of mammalian adenylyl cyclase. *J. Biol. Chem. 272*, 22265–22271.
32. Tesmer, J. J. G., Sunahara, R. K., Fancy, D. A., Gilman, A. G., and Sprang, S. R. (2002) Crystallization of comlex between soluble domains of adenylyl cyclase and activated Gsalpha. *Methods Enzymol.* 198–206.

33. Mou, T. C., Gille, A., Fancy, D. A., Seifert, R., and Sprang, S. R. (2005) Structural basis for the inhibition of mammalian membrane adenylyl cyclase by 2′(3′)-O-(N-methylanthraniloyl)-guanosine 5′-triphosphate. *J. Biol. Chem. 280*, 7253–7261.
34. Linse, S. (2002) Calcium binding to proteins studied via competition with chromophoric chelators. *Methods Mol. Biol. 173*, 15–24.
35. Otwinowski, Z., and Minor, W. (1997) Processing of x-ray diffraction data collected in oscillation mode. *Methods Enzymol. 276*, 307–326.
36. Brünger, A. T., Adams, P. D., Clore, G. M., Gros, P., Grosse-Kunstleve, R. W., Jiang, J.-S., Kuszewski, J., Nilges, M., Pannu, N. S., Read, R. J., Rice, L. M., Simonson, T., and Warren, G. L. (1998) Crystallography and NMR system (CNS): A new software suite for macromolecular structure determination. *Acta Crystallogr. D54*, 905–921.
37. Murshudov, G. N., Vagin, A. A., and Dodson, E. J. (1997) Refinement of macromolecular structures by the maximum-likelihood method. *Acta Crystallogr., Sect. D: Biol. Crystallogr. 53*, 240–255.
38. Collaborative computational project, N. (1994) The CCP4 Suite: programs for protein crystallography. *Acta Crystallogr. D50*, 760–763.
39. Read, R. J. (1986) Improved Fourier coefficients for maps using phases from partial structures with errors. *Acta Crystallogr. A42*, 140–149.
40. Jones, T. A., Zou, J. Y., Cowan, S. W., and Kjeldgaard, M. (1991) Improved methods for the building of protein models in electron density maps and the location of errors in these models. *Acta Crystallogr. A47*, 110–119.
41. Emsley, P., and Cowtan, K. (2004) Coot: model-building tools for molecular graphics. *Acta Crystallogr., Sect. D: Biol. Crystallogr. 60*, 2126–2132.
42. Alvarez, R., and Daniels, D. V. (1990) A single column method for the assay of adenylate cyclase. *Anal. Biochem. 187*, 98–103.
43. Alvarez, R., and Daniels, D. V. (1992) A separation method for the assay of adenylylcyclase, intracellular cyclic AMP, and cyclic-AMP phosphodiesterase using tritium-labeled substrates. *Anal. Biochem. 203*, 76–82.
44. Boyajian, C. L., Garritsen, A., and Cooper, D. M. (1991) Bradykinin stimulates Ca^{2+} mobilization in NCB-20 cells leading to direct inhibition of adenylylcyclase. A novel mechanism for inhibition of cAMP production. *J. Biol. Chem. 266*, 4995–5003.
45. Ahlijanian, M. K., and Cooper, D. M. (1987) Antagonism of calmodulin-stimulated adenylate cyclase by trifluoperazine, calmidazolium and W-7 in rat cerebellar membranes. *J. Pharmacol. Exp. Ther. 241*, 407–414.
46. Salomon, Y., Londos, C., and Rodbell, M. (1974) A highly sensitive adenylate cyclase assay. *Anal. Biochem. 58*, 541–548.
47. Segel, I. (1975) *Enzyme Kinetics: Behavior and Analysis of Rapid Equilibrium and Steady-State Enzyme Systems*, John Wiley & Sons, New York.
48. Sunahara, R. K., Beuve, A., Tesmer, J. J. G., Sprang, S. R., Garbers, D. L., and Gilman, A. G. (1998) Exchange of substrate and inhibitor specificities between adenylyl and guanylyl cyclases. *J. Biol. Chem. 273*, 16332–16338.
49. Tucker, C. L., Hurley, J. H., Miller, T. R., and Hurley, J. B. (1998) Two amino acid substitutions convert a guanylyl cyclase, RetGC-1 into an adenylyl cyclase. *Proc. Natl. Acad. Sci. U.S.A. 95*, 5993–5997.
50. Strynadka, N. C. J., and James, M. N. G. (1989) Crystal structures of the helix-loop-helix calcium-binding proteins. *Annu. Rev. Biochem. 58*, 951–998.
51. Tang, W. J., Stanzel, M., and Gilman, A. G. (1995) Truncation and alanine-scanning mutants of type I adenylyl cyclase. *Biochemistry 34*, 14563–14572.
52. Yan, S.-Z., Huang, Z.-H., Shaw, R. S., and Tang, W.-J. (1997) The conserved asparagine and arginine are essential for catalysis of mammalian adenylyl cyclase. *J. Biol. Chem. 272*, 12342–12349.
53. Tesmer, J. J., Dessauer, C. W., Sunahara, R. K., Murray, L. D., Johnson, R. A., Gilman, A. G., and Sprang, S. R. (2000) Molecular basis for P-site inhibition of adenylyl cyclase. *Biochemistry 39*, 14464–14471.
54. Mou, T. C., Gille, A., Suryanarayana, S., Richter, M., Seifert, R., and Sprang, S. R. (2006) Broad specificity of mammalian adenylyl cyclase for interaction with 2′,3′-substituted purine- and pyrimidine nucleotide inhibitors. *Mol. Pharmacol. 70*, 878–886.
55. Steitz, T. A. (1993) DNA- and RNA-dependent DNA polymerases. *Curr. Opin. Struct. Biol. 3*, 31–38.
56. Sutton, R. B., and Sprang, S. R. (1998) Crystal structure of the calcium-dependent phospholipid binding domain from protein kinase C-β in a ternary Ca^{2+} complex. *Structure 6*, 1395–1405.
57. Jaiswal, B. S., and Conti, M. (2003) Calcium regulation of the soluble adenylyl cyclase expressed in mammalian spermatozoa. *Proc. Natl. Acad. Sci. U.S.A. 100*, 10676–10681.
58. Litvin, T. N., Kamenetsky, M., Zarifyan, A., Buck, J., and Levin, L. R. (2003) Kinetic properties of "soluble" adenylyl cyclase. Synergism between calcium and bicarbonate. *J. Biol. Chem. 278*, 15922–15926.
59. Steegborn, C., Litvin, T. N., Levin, L. R., Buck, J., and Wu, H. (2005) Bicarbonate activation of adenylyl cyclase via promotion of catalytic active site closure and metal recruitment. *Nat. Struct. Mol. Biol. 12*, 32–37.

BI802122K